Int. J. Electrochem. Sci., 11 **(2016)** 2525 - 2533

International Journal of
ELECTROCHEMICAL
SCIENCE
www.electrochemsci.org

Facile Synthesis of MnO_2 Nanoparticles Well-dispersed on Graphene for the Enhanced Electrochemical Performance

Yanhong Zhao[1,2], Gang Chen[1,], DaWang[2], Chunlai Song[2], Liping Xie[2], Liang Chang[2], Rui Wang[1], Nailiang Zhong[2],*

[1] Department of Chemistry, Harbin Institute of Technology, Harbin 150001, China.
[2] College of Enviromental and Chemical Engineering, Heilongjiang University of Science and Technology, Harbin 150022, China
[*]E-mail: gchen@hit.edu.cn

Received: 17 September 2015 / *Accepted:* 19 October 2015 / *Published:* 1 March 2016

Graphene/MnO_2 (GN/MnO_2) composites have been facile synthesized *via* a liquid phase route. The results of the morphology reveal that MnO_2 nanoparticles about 20 nm are will-dispersed on the surface of the graphene nanosheets. The stable structure, through promoting the interfacial electron and lithium ion transport, improve the electrochemical performance of GN/MnO_2 with increasing 80% of the special capacity. The graphene in the composite accommodate volume change and increase electrical conductivity. Meanwhile the MnO_2 nanoparticles prevent the stacking of the graphene sheets, maintaining the stability of the GN/MnO_2 composites. So the stable characteristic structure by facile liquid phase route can be employed for other metal oxide composites of electrode or photocatalysis materials.

Keywords: graphene, MnO_2, lithium ion batteries

1. INTRODUCTION

The efficient energy storage and conversion technologies are necessary for extensive use of renewable energy. Some application such as portable electric vehicles and hybrid electric vehicle can meet the need of our information rich, mobile society. So the lithium ion batteries(LIBs), the noted electrochemical systems for energy storage and conversion, are pursued by many peoples [1-2]. But the commercially used graphite, based on the formation of LiC_6, ownes the theoretical capacity of 372 mA h g^{-1} [3]. It is too low to hamper its wide usage for LIBs in the surging consumer electronic devices, which can not satisfied for the market of renewable power applications. So it is imperative to explore new electrode materials and novel designs for higher energy density, lower cost, flexibility, non-toxicity, and better stability [4].

One approach of increasing lithium storage capacity is to use high theoretical capacities anode materials. Some oxidates, SnO_2, FeO, Co_3O_4 and NiO have been widely researched due to their higher theoretical capacities (>600 mA h g^{-1}) compared with the commercial graphite anode material(372 mA h g^{-1}). In particular, MnO_2 are stable, nontoxic and environmentally benign, and have a high specific capacity (>1230 mA h g^{-1}). Much effort is thus devoted to synthesize and control the structure of MnO_2-based materials [5-7]. However, the performance of MnO_2-based anodes remains inferior due to two main issues: (i) the pristine MnO_2 has a low electrical conductivity (10^{-5}–10^{-6} S/cm) which limits the electron transport; (ii) a large volume change of MnO_2 occurs during the lithiation and delithiation processes, which leads to severe electrode crush, serious safety concerns and rapid loss of discharge capacity during the cycling [7,8].

The orthohexagonal structure of graphene, made of sp^2 bonded carbon atoms, have attracted a lot of researchers. Graphene has been extensively used in physics, chemistry and materials science because of its good conductivity, well flexibility and special machanical property [9]. Yoo et al. investigated the graphene nanosheets (GNS) as the electrode materials for LIBs and the enhanced lithium storage capacity in 2008 [10]. The charge capacity of GNS was 540 $mAhg^{-1}$ at beginning, and the capacity increased up to 730 mA h $g^{-1}$and 784 mA h g^{-1}. The author explained the results attributing to graphene's unique structural of high surface area, better electric, chemical stability and thermal conductivity. Because of this, graphene has been used as perfect frameworks for graphenen-based composites as potential electrode materials [11]. Furthermore, Cui and co-workers has reported the study for Fe_3O_4 nano-particles attached onto the reduced graphene oxide sheets *via* a two-step hydrothermal method. The composite of Fe_3O_4/reduced graphene oxide has a improved rate capability compared with the bare Fe_3O_4 nanoparticles as the anode materials for LIBs [12].

In this work, the hybrid nanostructure graphene/MnO_2 (GN/MnO_2) is fabricated using a simple and environmentally-benign liquid method. The structure and morphology of prepared MnO_2 and GN/MnO_2 composite are observed, and their electrochemistry phenomenon are analyzed. We demonstrate that stable GN/MnO_2 composite exhibit enhanced electrochemical capability, comparing with the pure MnO_2. The GN/MnO_2 composite can be used a promising alternative anode material for lithium ion batteries.

2. EXPERIMENTAL & METHODS

2.1 Sample preparation

All chemicals were of analytical grade and were used without further purification unless otherwise specified. The synthesis process showed in Fig.1. First, GN were got by chemical reduction of the graphene oxide (GO) by hydrazine hydrate. GO nanosheets were prepared from nature graphite powders by using a modified Hummers method reported previously [13]. Then, graphene/MnO_2 composites were prepared with in situ MnO_2 deposition on the surface of graphene *via* a simple one-step liquid method. 50 mg GN and 0.22 g $Mn(Ac)_2$ were dissolved in 100 ml distilled water under the condition of constantly stirring. The 26 mg $KMnO_4$ (dissolved in 10 ml distilled water) was slowly

added into the above solution, then continuously stirred for 2 h. The precipitate was obtained and washed for 5 times, last dried at 60 ^{o}C under vacuum for 6 h. In this way, the MnO_2/graphene composites powders were synthesized. The MnO_2 without GN were prepared with above method for comparison.

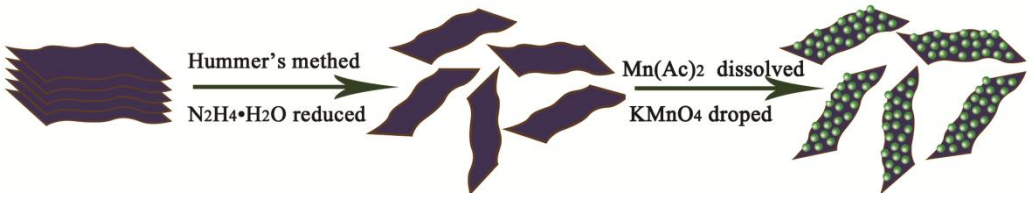

Figure 1. Schematic of the Formation of GN/MnO_2 Composites**.**

2.2 Material characterization

X-ray diffraction (XRD) patterns were obtained by a Bruker D-8 advanced X-ray diffractometer with Cu Kα radiation (λ = 0.15418 nm) in the range of $10^{o} \leq 2\theta \leq 70^{o}$. Scanning electron microscope (SEM) and transmission electron microscope (TEM) images were received, through a SEM (Quanta 200F) with an acceleration voltage of 3 kV and a TEM (JEM-2010FEF) with an acceleration voltage of 200 kV, respectively. X-ray photoelectron spectroscopy(XPS) tests were carried out on a PHI 5700 XPS/ESCA system with a monochromatic Al Kα (1486.6 eV).

2.3 Preparation of lithium-ion batteries

Electrochemical performances of graphene, MnO_2 nanoparticles and GN/MnO_2 composites were investigated with coin-type cells (CR2025). The working electrodes were prepared by a slurry (80 wt% active material, 10 wt% polyvinylidene fluoride (PVDF) in N-methyl pyrrolidone (NMP), and 10 wt% carbon black) coating procedure. Test cells were assembled in an argon-filled glove box with the metallic lithium foil as the reference and counter electrodes. The electrolyte was 1.0 mol dm^{-3} $LiPF_6$ in a mixture of ethylene carbonate (EC) and dimethyl carbonate (DMC). The galvanostatically charged and discharged were measured in the range of 0.01–3.0V (*vs.* Li/Li^{+}) at room temperature using a NEWWARE battery test system. AC impedance measurement was carried out using a CHI604C (Shanghai Huachen Electronics Ltd.) electrochemical working station in the 100 KHz to 10mHz frequency range.

3. RESULTS AND DISCUSSION

XRD patterns of graphene and graphene/MnO_2 are shown in Fig.2. In the pattern, all the peaks of GN/MnO_2 hybrid and MnO_2 are distinguishable. The diffraction angles at 12.84^{o},18.28^{o},28.84^{o}, 37.66^{o}, 41.88^{o}, 49.78^{o}, 56.18^{o}, 60.34^{o}, 65.72^{o} and 69.34^{o}, can be assigned to (110), (200), (310), (211),

(301), (411),(600), (521), (002) and (541) crystal planes of a pure tetragonal α-MnO_2 phase (JCPDS, No. 44-0141), respectively. The XRD peak positions and shapes of GN/MnO_2 are similar with those of MnO_2, diffraction peaks of GN are not obviously observed. It may be the mass ratio of GN is little and the peaks of GN and MnO_2 about at 18^o to 27^o are overlapping. The diffraction peaks of GN would weaken even vanish as reported because the regular stacks of GN could be separated by inorganic unites [14, 15].

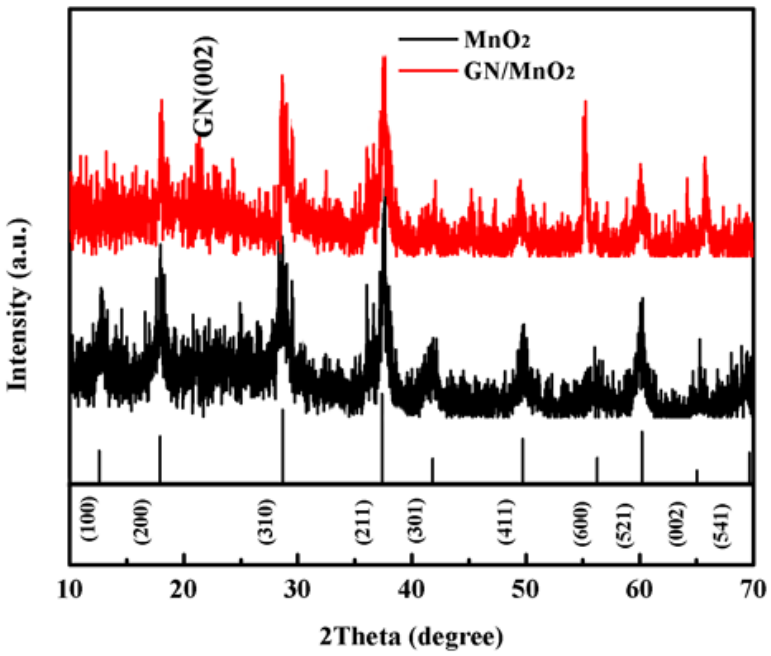

Figure 2. XRD pattern of MnO_2 and GN/MnO_2.

The images of Fig. 3(a) further illustrates the present of MnO_2 on the graphene surfaces. X-ray photoelectron spectroscopy (XPS) spectra of C1s, O1s and Mn2p orbitals of the GN/MnO_2 hybrid are shown in Fig. 3. The Mn2p spectrum of GN/MnO_2 composite is presented in Fig. 3(b), where the peaks of $Mn2p_{3/2}$ (642.1 eV) and $Mn2p_{1/2}$ (653.7 eV) are observed. They have a spin energy separation of 11.6 eV in good accordance with the reported datum on MnO_2[16], which ensures the presence of MnO_2 in the composite. Fig. 3(c) shows the pure spectra of C1s, which can be suited as two peaks at binding energies of 284.6 and 288.4 eV, meaning two different chemical valencies of carbon existing in the sample. The peaks at 284.6 eV can be assigned to contributions of C-C (sp^2) bonds [17]. While the peak at 288.4 eV comes from the existence of C-OOH bonds [18]. It can be attribute that GN is the reduction product of graphene oxide. Fig. 3(d) shows the high resolution spectra of O1s. In the case of GN/MnO_2 hybrid, the curve fitting of O1s peak basically indicates two components centered at 529.6 and 531.3 eV. The O1s peak at 529.6 eV is assigned to the oxygen bonded with manganese (Mn-O) in MnO_2 crystal lattice [19]. The another peak is obviously ascribed to the surface hydroxide radical of carbon phase [20].

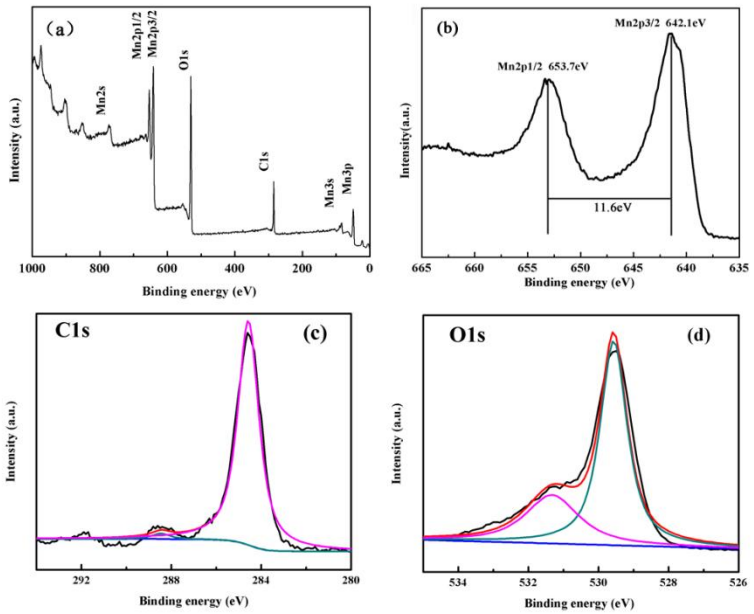

Figure 3. XPS spectra measured at the surface of GN/MnO_2 composites.

The morphology images of MnO_2, GN/MnO_2 composites and GN are shown in Fig. 4. Pure MnO_2 was prepared by liquid phase method at room temperature. From Fig. 4(a), the diameters of the MnO_2 nanoparticles range about 100 nm, and the morphologies of MnO_2 are in good agreement with reported data [21]. The particle of MnO_2 has the reunited phenomenon, while the particle on the surface of graphene (Fig. 4(b)) is homogeneous. Fig. 4(c) is the image of the graphene after chemical reduction, and the graphene exhibite the morphology similar to thin silk. It has a large flat surface which could avail for anchoring the MnO_2. And it can work as the buffer limiting the volume change when the electrochemistry reactions occur.

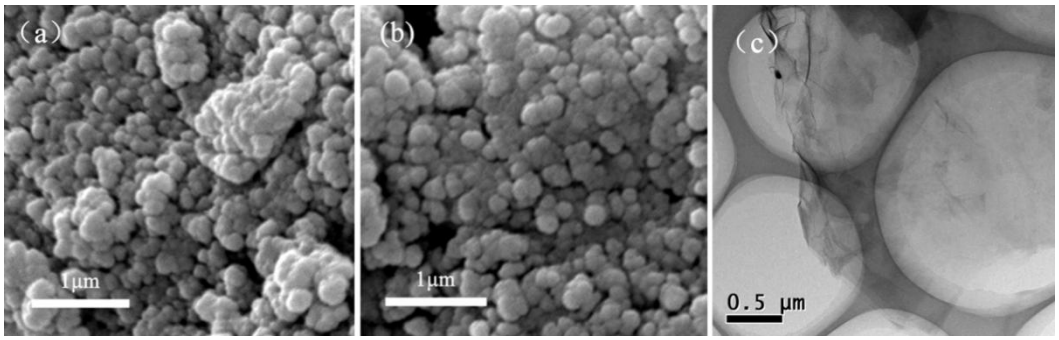

Figure 4. SEM images of MnO_2 (a), GN/MnO_2 composite (b)and TEM images of GN (c).

The TEM and HRTEM images of the GN/MnO_2 composites are shown in Fig. 5. It is clear that many MnO_2 nanoparticles about 20 nm anchored on the surface of graphene and the MnO_2 particles disperse homogenously (Fig. 5(a)). The structure of well-dispersed nanoparticles on the graphene will provide large surface area.

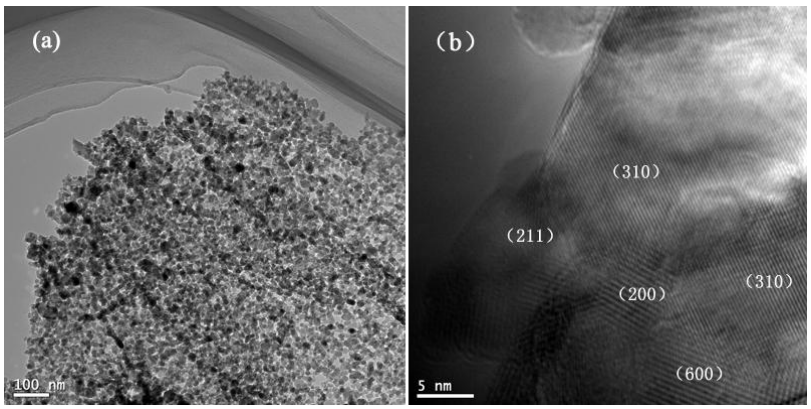

Figure 5. TEM and HRTEM images of GN/MnO_2.

Meanwhile, the stable three-dimensional structure is constructed by particle MnO2 and graphnene sheets which would restrict the stacking and accumulating of graphene and keep the strong structure. So the well-distributed particles can provide clear and coherent path of Li^+ transportation and more exposed surface which would promote the Li^+ diffusion. The HRTEM image of Fig. 5(b) reveals the crystal feature of MnO_2 nanopaticle and clear lattice fringes of well-crystallized MnO_2. The distances between the two fringes are 0.31 nm, 0.49nm, 0.16nm, 0.24nm respectively, corresponding to the (310), (200)，(600), (211) lattice planes [22]. All these images could present the uniformity structure of the composite which is reasonable for the enhanced capacity.

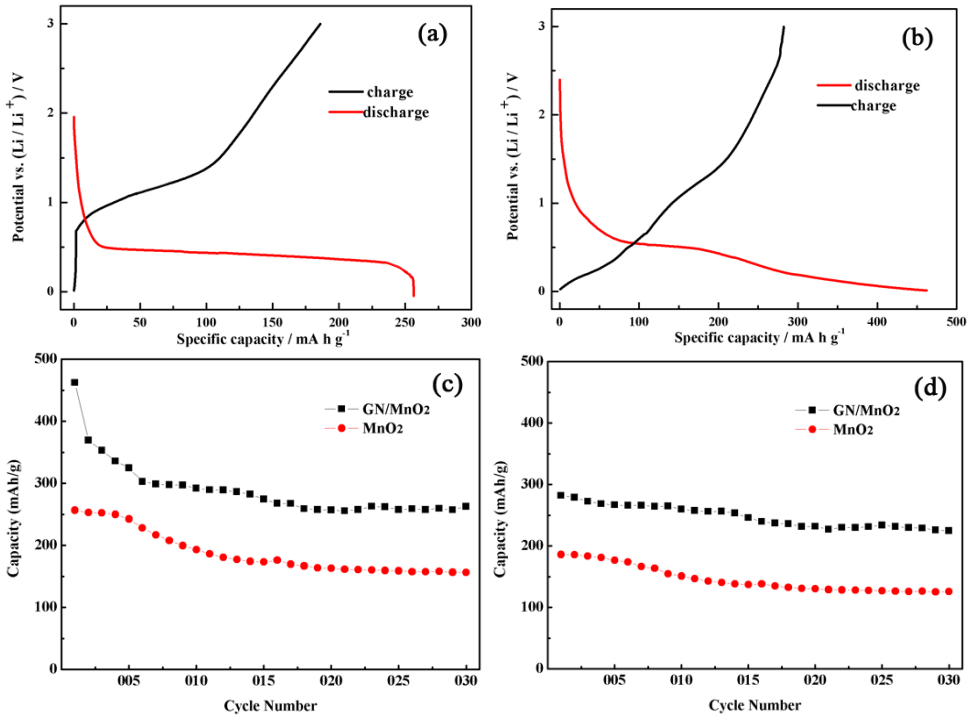

Figure 6. the first Galvanostatic Discharge/charge Curves for MnO_2 (a) and GN/MnO_2 composite (b); Capacity *vs.* cycle number at 100mA/g for MnO_2 and GN/MnO_2 composite; (c) discharge capacity; (d) charge capacity.

To confirm the improving effect of the GN/MnO_2 for the electrochemical perfromance, The charge and discharge voltage profiles of the MnO_2 and GN/MnO_2 were got by using half-cell test as anode materials. The rate capability was tested using the same method. Fig. 6(a) and (b) is the charge/discharge curves of MnO_2 and GN/MnO_2 nanocomposites in the 1st cycles, respectively. The discharge curves of MnO_2 and GN/MnO_2 have the same plateau at the voltage of 0.7 V. This can be explained that the solid electrolyte interface (SEI) layer is formed and the electrolyte is decomposed on the electrode surface [23]. The platform at 0.5 V can be surveyed in the following discharge processes by GN/MnO_2 and MnO_2. It shows that the initial discharge/charge capacity of GN/MnO_2 at the rate of 100mA g^{-1} is 462.22 and 282.25 mA h g^{-1}, respectively. That of MnO_2 is 256.53 and 186.03 mA h g^{-1}, respectively. The capacity of GN/MnO_2 composite is higher than that of MnO_2, enhanced 205.69 mA h g^{-1}. Fig. 6(c) and (d) show the cyclability of MnO_2 and GN/MnO_2 composites. From Fig. 6(c), it can be seen that the discharge capacity after 30 cycles of GN/MnO_2 composites maintain 262.29 mA h g^{-1}, but the capacity of MnO_2 is 156.45 mA h g^{-1}. As shown in Fig. 6(d), the charge capacity after 30 cycles of GN/MnO_2 is 224.50 mA h g^{-1} which is nearly double times compared with capacity of MnO_2. Such a enhanced performance can be ascribed to the following points. One is the uniform size of nanopaticles and MnO_2 nanopaticles well-distributed on the graphene, which may reduce the heaped up of graphene sheets and provide the high surface area. This stable structure could come into being stable route for Li^+ transmission in charge/discharge process. Another is graphene that has the high electrical conductivity which facilitates electrons transporting from graphene to MnO_2 nanostructures. And the excellent flexibility of graphene would limit and remit the volume change of enlarging or shrinking at the process of lithium embedded in and out [24].

Fig.7 depicts the Nyquist plots of MnO_2 nanoparticles and GN/MnO_2 composties. The semicircle in the middle frequency range indicates the charge and discharge transfer resistance [25]. It can be clearly seen that the charge and discharge transfer resistance of GN/MnO_2 electrode is smaller than MnO_2. This explains the enhanced performances of composite material at lithium ion diffusion and the electronic transmitting thus enhancing the lithium storage capacity. More importantly, the uniform size and well-distributed MnO_2 nanopaticles may relieve the stacking of graphene sheets and keep the high surface area. Consequently, the lithium storage capacity and the cycling performance of GN/MnO_2 composite can be enhanced.

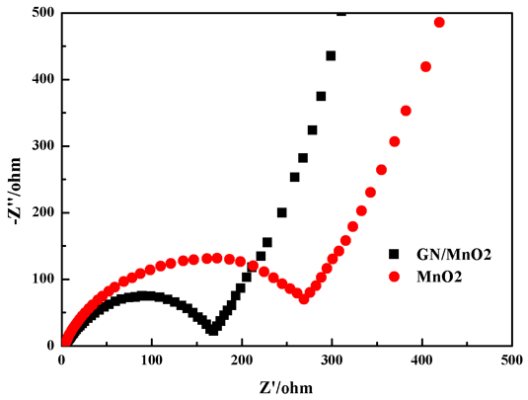

Figure 7. Electrochemical impedance results of MnO_2 and GN/MnO_2 electrodes.

4. CONCLUSION

In summary, the GN/MnO_2 composite is prepared as an anode for lithium ion battery *via* a liquid phase route. The homogenous MnO_2 nanoparticles about 20 nm anchored on the surface of graphene. The composite has high specific capacity of 462.22mA h g^{-1} at 100mA g^{-1}. And after 30 cycles, the capacity of GN/MnO_2 is nearly double times compared with the capacity of MnO_2. The enhanced electrochemical performance is due to the integration of graphene and MnO_2. They formed the stable hybrid structure of homogeneous MnO_2 nanopaticles well-dispersed on the graphene surface, the structure not only increases the contact area facilitating electrochemistry reaction between Li^+ and the electrode but also reduces the resistance in charge and discharge process. Another, the graphene acts as the conductive link for electron transport, the MnO_2 nanostructures support graphene laryer from stacking. The suitable structures of the prepared composite enhance the diffusion of electrons and the transfer of lithium ions. At last, the electrochemical performances of the GN/MnO_2 are impoved. The prepared method can be extended for other metal oxide, and the stable structure constructed by graphene will be a alternative for the composites.

ACKNOWLEDGEMENTS
This work was financially supported by projects of Natural Science Foundation of China (21271055 and 21471040), China Postdoctoral Science Foundation funded project (2015M570298) and the project of Youth Science Foundation of Heilongjiang Province in China (No.QC2012C079).

References

1. Y. M. Chiang, *Science*, 330 (2010) 1485.
2. Y. Y. Lu, K. Korf, Y. Kambe, Z. Y. Tu, and Lynden A. Archer, *Angewandte Chemie*, 126 (2014) 498.
3. J. M. Tarascon , and M. Armand , *Nature*, 414 (2001) 359.
4. R. Shapira, G. D. Nessim, T. Zimrin, and D. Aurbach, *Energy& Environmental Science* , 6 (2013) 587.
5. P. Poizot, S. Laruelle, S. Grugeon, L. Dupont, and J-M. Tarascon, *Nature*, 407 (2000) 496.
6. T. T. Truong, Y. Z. Liu, Y. Ren, L. Trahey, and Y. G. Sun, *ACS Nano*, 6 (2012) 8067.
7. A. P. Yu, H. W. Park, A. Davies, D. C. Higgins, Z. W. Chen, and X. Cheng, *Journal of Physical Chemistry Letter*, 2 (2011) 1855.
8. J. C. Guo, Q. Liu, C. S. Wang, and M. R. Zachariah, *Advanced functional Materials*, 22 (2012) 803.
9. A. K. Geim, and K. S. Novoselov, *Nat. Mater.*, 6 (2007) 183.
10. E. J. Yoo, J. Kim, E. Hosono, H. S. Zhou, T. Kudo, and I. Honma , *Nano Lett.*, 8 (2008) 2277.
11. K. M. F. Shahil, and A. A. Balandin, *Solid State Commun.*, 152 (2012) 1331.
12. H. L. Wang , L. F. Cui, Y. Yang, H. S. Casalongue, J. T. Robinson, Y. Y. Liang, Y. Cui, and H. J. Dai, *J. Am. Chem. Soc.*, 132 (2010) 13978.
13. W. S. Hummers Jr. and R. E. Offman, *Journal of the American Chemical Society*, 80 (1958) 1339.
14. L. Qiu, X. Yang, X. Gou, W. Yang, Z. F. Ma, G. G. Wallace, and D. Li, *Chem.-Eur. J.*, 16 (2010) 10653.
15. R. Pasricha, S. Gupta, and A.K. Srivastava, *Small*, 5 (2009) 2253.
16. Z. B. Lei, F. H. Shi, and L. Lu. *ACS Appl Mater Interface*, 4 (2012) 1058.

17. R. Bhowmick, S. Rajasekaran, D. Friebel, C. Beasley, L. Jiao, H. Ogasawara, H. Dai, B. Clemens and A. Nilsson, *Journal of the American Chemical Society*, 133 (2011) 5580.
18. Q. Xiang, J. Yu, and M. Jaroniec, *Nanoscale*, 3 (2011) 3670.
19. Q.T. Qu, P. Zhang, B. Wang, Y.H. Chen, S. Tian, Y.P. Wu, and R. Holze, *J. Phys. Chem. C*, 113 (2009) 14020.
20. Q.J. Xiang, J.G. Yu, and M. Jaroniec, *J. Phys. Chem. C*, 115 (2011) 7355.
21. B. Ming, J. Li, F. Kang, G. Pang, Y. Zhang, and X. Wang, et al., *Journal of Power Sources*, 198 (2012) 428.
22. J. Zhu, W. Shi, N. Xiao, X. Rui, H. Tan, X. Lu, H.H. Hng, J. Ma, and Q. Yan, *ACS Appl. Mater. Interf.*, 4 (2012) 2769.
23. T. Li, and L.J. Gao, *Journal of Solid State Electrochemistry*, 16 (2012) 557.
24. J. X. Zhu , D. Yang , Z. Y. Yin , Q. Y Yan , and H. Zhang, *Small*, 2014, DOI: 10.1002/small 201303202.
25. Y. J. Mai, X. L. Wang, J. Y. Xiang, Y. Q. Qiao, D. Zhang, C. D. Gu, and J. P. Tu, *Electrochimica Acta*, 56 (2011) 2306.